physics

MDPI

Review

Trends in the Structure of Nuclei near ^{100}Sn

Magdalena Górska

GSI Helmholtzzentrum für Schwerionenforschung GmbH, D-64291 Darmstadt, Germany; m.gorska@gsi.de

Abstract: Inevitable progress has been achieved in recent years regarding the available data on the structure of ^{100}Sn and neighboring nuclei. Updated nuclear structure data in the region is presented using selected examples. State-of-the-art experimental techniques involving stable and radioactive beam facilities have enabled access to those exotic nuclei. The analysis of experimental data has established the shell structure and its evolution towards $N = Z = 50$ of the number of neutrons, N, and the atomic number, Z, seniority conservation and proton–neutron interaction in the $g_{9/2}$ orbit, the super-allowed Gamow–Teller decay of ^{100}Sn, masses and half-lives along the rapid neutron-capture process (r-process) path and super-allowed α decay beyond ^{100}Sn. The status of theoretical approaches in shell model and mean-field investigations are discussed and their predictive power assessed. The calculated systematics of high-spin states for $N = 50$ isotopes including the 5^- state and $N = Z$ nuclei in the $g_{9/2}$ orbit is presented for the first time.

Keywords: nuclear structure; shell model; magic nuclei; gamma-ray spectroscopy

check for updates

Citation: Górska, M. Trends in the Structure of Nuclei near ^{100}Sn. *Physics* **2022**, *4*, 364–382. https://doi.org/10.3390/physics4010024

Received: 26 November 2021
Accepted: 2 March 2022
Published: 21 March 2022

Publisher's Note: MDPI stays neutral with regard to jurisdictional claims in published maps and institutional affiliations.

1. Introduction and Ground-State Properties

The $N = Z = 50$ nucleus ^{100}Sn, with N being the number of neutrons and Z being the atomic number, is the heaviest self-conjugate and doubly-magic nucleus that remains stable with respect to heavy-particle emission and thus provides an excellent opportunity for shell-model studies. In particular, its unique placement in the chart of nuclei makes it and its neighbors the most suitable to investigate neutron–proton correlations based on the coupling of single particle states with respect to a doubly-magic-core. However, in view of these advantages, the progress on the relevant experimental information in this region is moderate in spite of enormous efforts of physicists around the globe.

It directly relates to the accessibility of these nuclei in any known production reaction and therefore also to technical accelerator developments. Recent related technical developments have a large impact on this field. The history of the approaches to investigate ^{100}Sn was addressed in the latest review [1] where the experimental and theoretical status of the region was summarized until 2013. The purpose of this work is to report on recent developments in this region relevant for the understanding of the nuclear force.

The ^{100}Sn ground state is expected to be bound by about 3 MeV with respect to proton emission [2], which makes its yrast states accessible to γ-ray spectroscopy. The proton dripline was recently predicted [3] to be at $N = 47$ for the element of tin. The first ab initio prediction for the charge radius and density distribution of ^{100}Sn was attempted in Ref. [4]. The latest example of experimental developments to study nuclear size in this region is given in Ref. [5]. In-gas-cell laser ionization spectroscopy and extraction of magnetic moments and mean-square charge radii of light Ag isotopes was presented in Ref. [6].

The strength of the Super Gamow-Teller transition [7], $B(GT)$ from the ground state of ^{100}Sn, which could yield the largest value observed within the electron capture (EC) decay energy, Q_{EC}, window in the whole chart of nuclei, was originally predicted in Ref. [8]. It was measured for the first time by Hinke et al. [9]. Significant progress was obtained since then as the experimental value was revisited recently [10] and discussed theoretically in [11–14]. The two experimental $B(GT)$ values, originating from beta decay process, differ significantly.

This is mainly caused by the greatest deficiency of the beta-decay spectroscopy measurements that is the determination of Q_{EC}, i.e., $Q_{\beta,}$ which is needed for extraction of $B(GT)$ value. The reason for that is a strong dependence of phase-space factor f on the decay energy. This calls for a high-precision mass measurement of ^{100}Sn. Indeed, also here the progress is significant. Mass measurements in the region were recently extended [15,16], suggesting that the Q_{EC} of Ref. [9] to be more consistent with those new results. The mass of ^{100}Sn itself is likely within reach very soon.

The first possible excited yrast states in ^{100}Sn are particle-hole excitations of the closed core. No excited states of ^{100}Sn were reported thus far, as shown in Figure 1. To address directly the structure of ^{100}Sn itself, an extended work has been invested into calculations of both α-cluster formation and decay probabilities in ideal heavy α emitters ^{104}Te and the ^{212}Po for a direct comparison [16]. In this microscopic calculation of α-cluster formation with an improved treatment of shell structure for the core nucleus, it was found out that the effective potential is sensitive to the contributing single-particle wave functions.

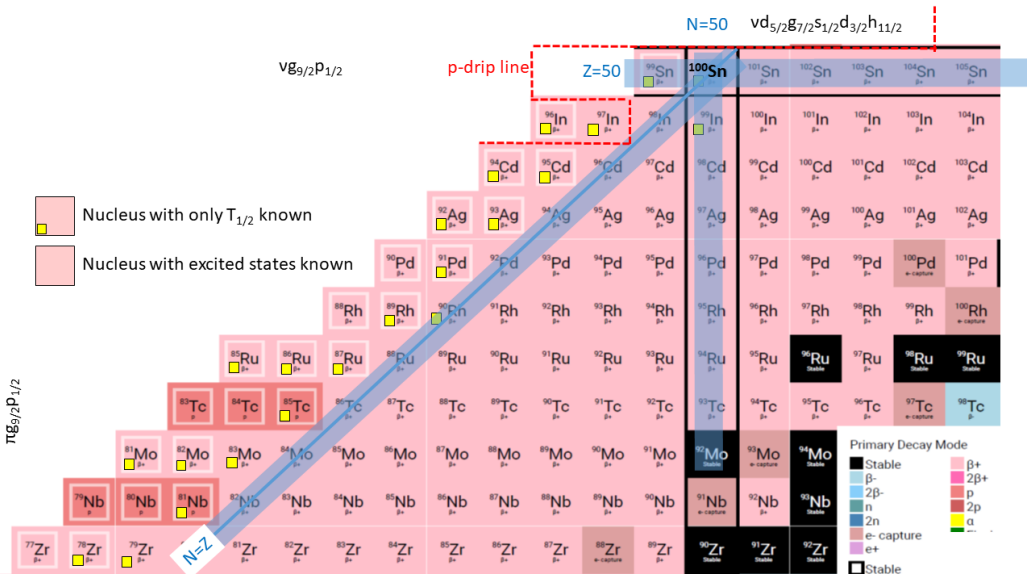

Figure 1. Present status of experimental information on the ground-state lifetime and excited states in the ^{100}Sn region. Nuclei with only the ground-state lifetime known and no excited states reported are indicated with a small yellow square. The nuclei to the left of them were only produced in an experiment. The blue-shaded chains of nuclei highlight the main focus of this review.

Striking shell effects on the α-cluster formation probabilities are shown for magic numbers 50, 82 and 126 by using the same nucleon-nucleon interaction. An enhanced α-cluster formation probability was shown for both ^{104}Te and ^{212}Po as compared with their neighbors. In Ref. [17], a particular enhancement in the ^{100}Sn region was suggested with respect to that in ^{208}Pb. The analysis of the statistical significance of the neutron skin thickness to the symmetry energy in ^{132}Sn and comparison to proton skin in ^{100}Sn was performed by Muir et al. [18]. As in the first case, a clear correlation was observed for neutron skin, in the later no correlation could be deduced for ^{100}Sn.

The nuclear structure of hole states in the region "southwest" of the shell closure at ^{100}Sn, close to the $N = Z$ line is dominated by the $g_{9/2}$ intruder orbital from the $N = 4$ harmonic oscillator (HO) shell. This is well separated from the $N = 3$, *pf* orbitals, both energetically and by parity, allowing only $2p$-$2h$ excitations into the intruder orbital space. Dominated by the strong proton-neutron interaction, the $0g_{9/2}$ orbit gives rise to unique structural features [1] such as spin-gaps, seniority [19–21] and parity-changing isomerism [22] in addition to proton-neutron pairing correlations [23] and seniority-induced symmetries [24]. Moreover, when moving below $Z = 45$, deformation and shape coexistence of spherical and

deformed shapes start to appear. Therefore, the region "southwest" of ^{100}Sn has become and remains, the subject of ever-increasing efforts both in experiments and theory.

The $N = Z$ nuclei provide the best quantum laboratory to investigate the characteristics of the neutron–proton (*np*) interaction, isospin symmetry and mixing, in addition to evolution of nuclear shapes. The $N \approx Z$ nuclei up to the $A = 60$ mass region have been intensively investigated during the past twenty years in various laboratories around the world. Here, the nuclei have been experimentally accessible as they are located only few neutrons away from their stable isotopes. From the nuclear theory perspective, especially regarding the nuclear shell model, the $N \approx Z$ nuclei between the $A = 40$–60 mass region have been an ideal subject to study since the valence nucleons occupy primarily the $f_{7/2}$ orbital making the calculations feasible due to the small valence space.

Currently, experimental ground-state decay and nuclear structure data, such as the level schemes and lifetimes of excited states for the $N \approx Z$ nuclei around the $A = 60$–90 mass region, are relatively scarce. This is due to the fact that these nuclei are located further away from the line of stability, near the proton-drip line. The production cross sections of these systems in nuclear reactions are very low (tens of nb to few μb). The missing experimental data from this region is naturally required in order to scrutinize and develop theoretical models operating in larger model spaces. However, radioactive ion beams (RIB) in this region are becoming gradually available for experiments, which can be utilized in various ways to search for new physics around the $N = Z$ line.

The evolution of nuclear shell structure in the vicinity of doubly-magic nuclei is of major importance in nuclear physics. The Sn isotopes provide a unique testing ground in this respect. The Sn isotopes represent the longest chain of semi-magic nuclei in nature, which makes them attractive for systematic investigations. How the shell structure evolves as a function of the number of protons and neutrons can be related to collective as well to single-particle effects. Unique correlation effects may be manifested at a self-conjugate shell-closure as the same spin-orbit partners for neutrons and protons reside just above and below the shell gap.

A sensitive probe for correlations of this kind is to measure transition probabilities for certain selected states. With this approach the results of large-scale shell-model (LSSM) calculations based on microscopically-derived interactions can be tested through direct comparison with experiment. The study of simple nuclear systems, with only a few nucleons outside a closed core, can thus provide insight into the underlying nucleon-nucleon interaction as applied to finite nuclei.

This paper summarizes briefly the new results on the structure of excited states of nuclei in ^{100}Sn region and is organized as follows. After the general introduction including ground-state properties, the most successful experimental methods to obtain knowledge on excited states in nuclei in the region are elaborated in Section 2. Theoretical approaches are summarized briefly in Section 3.

The focus on new results of the shell-model calculations and their comparison to the recent experimental data is put in Section 4 for three sub regions describing certain symmetries shaded in blue in Figure 1. The $N = 50$ isotones are addressed in Section 4.1.1. The progress on $N = Z$ nuclear chain just below ^{100}Sn is described in Section 4.1.2. The recent results on light Sn isotopes and selected nuclei with $N > 50$ below Sn are presented in Section 4.2. The choice of presented data from recent experimental and theoretical results is based on the author's subjective taste.

2. Experimental Methods

Although a comprehensive summary of the experimental status in the ^{100}Sn region was reported in 2013 [1], the struggle to discover new aspects of structure of those nuclei continued. To assure progress in this very difficult to reach nuclear region, an enormous effort is devoted to the experimental techniques. Several aspects are crucial among the developments. The prerequisite is the availability of accelerators with beam parameters, i.e., energy and intensity etc., optimal for a given experimental apparatus.

Two types of experiments are distinguished with the highest impact on the progress obtained: low-energy facilities providing higher beam intensities for fusion and multi-nucleon transfer reactions and high energy facilities for fragmentation and spallation reactions producing radioactive beams, so called in-flight and isotope separation on-line (ISOL) facilities. While in earlier times the majority of experimental information was delivered from fusion-evaporation reactions at the low-energy facilities, recent years have shown the significance of the later ones.

2.1. Low Energy Facilities

Highly-intense beams of stable isotopes are available at several facilities such as GANIL (Large Heavy Ion National Accelerator, Caen, France) [25], Jyväskylä University [26], Argonne National Laboratory (ANL) [27] and INFN (National Institute for Nuclear Physics, Italy) Legnaro [28], to name only a few. These low-energy accelerators serving fusion-evaporation or multi-nucleon-transfer reactions newly-applied also in the ^{100}Sn region [29], play a very important role when combined with highly-efficient detectors.

Such a combination was recently available at GANIL [25] with AGATA [30,31] and ancillary detectors as e.g., DIAMANT [32,33] and NEDA [34,35], which make the exit channel identification possible. Alternatively, a recoil spectrometer such as VAMOS [36–38], MARA [39], or the FMA [40] may serve for residue identification. A clear advantage of this method is prompt spectroscopy at the reaction target tagged with identified recoils or a decay particle (e.g. γ, β, α).

Often, population of high-spin states, in particular in fusion-evaporation reactions, is considered advantageous. However, in the ^{100}Sn region the most exotic nuclei that can be investigated are produced in 2-neutron ($2n$) or more and $2n\alpha$ exit channels [41]. Those residues are produced with the highest cross section at relatively low energies above the Coulomb barrier keeping the total reaction cross section low in order to avoid misidentification due to contaminants. At those lower energies, the reached spin values and residue excitation energy are reduced.

Impressive experiments of this type were performed in the last years leading to important discoveries, e.g., the delayed rotational alignment in a deformed $N = Z^{88}$Ru [42]. Another way for the production of very neutron deficient Sn isotopes is alpha decay tagging measurements of the Te isotopes. The two leading groups at ANL with FMA [43,44] and at Oak Ridge National Laboratory (ORNL) [45,46] have been hunting for superallowed α-decay signatures for the last 15 years. The burning question—whether it is energetically possible to produce excited states in ^{100}Sn in this way—remains open [47].

2.2. High-Energy Fragmentation and ISOL Facilities

When the beam energy reaches the range suitable for fragmentation reactions, in-flight separation and identification of reaction products can be achieved. The lower beam intensities at high energies and lowered production cross sections are then compensated by the possibility of using thicker targets and higher efficiency of tracking and identification detectors. Unprecedented primary-beam intensities at relativistic energies have become available at the Radioactive Isotope Beam Factory (RIBF) at the RIKEN Nishina Center (Japan).

The reaction products are identified in the BigRIPS fragment separator [48] accompanied by an efficient γ-ray array, e.g., EURICA [49] (see Figure 2) consisting of EUROBALL cluster detectors for high-energy resolution or DALI2+ spectrometer [50] for low-resolution spectroscopy. Experiments of this type marked a new chapter in the available data in the ^{100}Sn region including the discovery of new isotopes and proton emitters [51]. An important add-on was the new measurement of the *B(GT)* value for ^{100}Sn β-decay measurement made with sufficient accuracy so that the interpretation allowed for distinguishing between different models used [10].

The existing data can be used for *B(GT)* re-determination once the mass measurement of ^{100}Sn is available. Extensive data on lifetimes of β decay and β-delayed proton

emission, as well as beta-delayed spectroscopy was published in Refs. [52,53]. Large progress on excited states in the region was obtained including gamma-gamma coincidence data for the ^{100}In nucleus [10], identification of excited states in ^{96}Cd [22,54] and others [55,56] based on isomer spectroscopy are mentioned in Section 4.1. The disadvantage of this method is that it does not allow for prompt gamma-ray spectroscopy at the (primary) target.

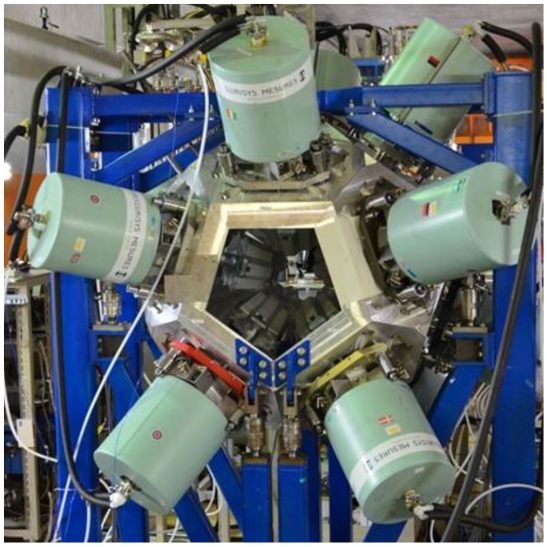

Figure 2. EURICA array consisting of 12 cluster detectors of EUROBALL at RIKEN RIBF in 2012 [49]. See text for details.

Two-step fragmentation is used to study prompt radiation from Coulomb excitation or knockout reactions with the DALI2+ spectrometer. From several experimental campaigns, extensive and spectacular data was collected and, to large extent, published as discussed in Section 4.2. Very recently, in 2020–2021 the HICARI (High-resolution in-beam gamma-ray spectroscopy at RIBF) project [57] used a Ge-detector array to perform several experiments addressing this region.

Efforts continue at NSCL (National Superconducting Cyclotron Laboratory, Michigan, USA) to contribute to the region [58], e.g., with spectroscopy using knock-out reactions [59], or the recent mass measurement of ^{80}Zr [60]. At GSI, revisited isomeric decay in ^{102}Sn and resulting effective neutron and proton charges based on state-of-the-art shell-model calculations were published [61], 13 years after the RISING [62] experiment.

In 2020, the GSI (Society for Heavy Ion Research, Darmstadt, Germany) facility came back into operation again after 6 years with the Fragement Separator (FRS) [63] and DEcay SPECtroscopy (DESPEC) [64] setup including the FATIMA [65] gamma-ray array and a Ge-detector array to address this region of nuclei again with lifetime measurement of intermediate states below isomers or states populated in beta decay.

To determine the excitation energy of long-lived isomeric states, a complementary technique employing the Multi-Reflection Time-of-Flight Mass Spectrometer (MR-TOF-MS) at the FRS Ion Catcher was recently used in this region of nuclei [15].

Alternatively, high-energy and high-intensity protons are used in spallation reaction and the radioactive beam is stored and separated in an ion source. Laser-ionized secondary beams are accelerated to fusion energies to impinge on a secondary target surrounded by a γ-ray array. The enormous success of this method was demonstrated at CERN (the European Organization for Nuclear Research) REX-ISOLDE [66] and continued with the HIE-ISOLDE project [67] where secondary beams were used for transfer and Coulomb-excitation measurements using the MINIBALL γ-ray array [68,69]. Several experiments were devoted to the study of neutron-deficient tin via transfer and Coulomb excitation measurements [70–74].

A similar principle was recently also applied at NSCL in [75] using the JANUS setup [76].

3. Theoretical Approaches

Similarly, theory activities in the ^{100}Sn region did not lose momentum in the years since the last review [1]. Indeed, several approaches ([61,77–84]) could enlarge the treated configuration space (truncation level) and/or go to new regions of the nuclidic chart for The LSSM calculations, which helped to explain certain phenomena not clarified before and suggested experiments for future studies. These calculations use mostly realistic interactions derived from a nucleon-nucleon potential with various treatments to obtain two-body matrix elements and single-particle energies as described for example in [1,83] and references therein.

On the other hand, the comparison of those advanced calculation results to the ones with a smaller model space and empirical interactions, which are doable in the scope of this review work, can shed light on certain basic principles, which were not treated yet with large codes and computer power. For this purpose, the empirical GF [85] and SLGT [86] interactions in the $p_{1/2}g_{9/2}$ model space is used here, with single-particle level energies adjusted as given in [1], to guide the basic understanding of the underlying structure.

In the scope of this work, JUN45 interaction [78] results in the $\pi\nu(f_{5/2},p_{3/2},p_{1/2},g_{9/2})$ (or r3*g*) model space for high spin states are also presented in Section 4 for several $N = 50$ isotones and $N = Z$ nuclei of the $g_{9/2}$ shell. The shell-model code NuShellX [87] was used for these computations. The MHJM interaction in the $\pi p_{1/2}g_{9/2}$ $\nu d_{5/2}g_{7/2}d_{3/2}s_{1/2}h_{11/2}$ model space originating from [88] was successfully used in the literature to describe the structure of nuclei with $Z \leq 50$ and $N \geq 50$ [89], see e.g., [1,53,90,91]. The LSSM calculations in the e.g., [61,92,93] with the SDG interaction [22] for the $\pi\upsilon(g_{9/2},d_{5/2},g_{7/2},s_{1/2},d_{3/2})$ model space (further referred as *gds*) are described in more detaill below.

Recently, new approaches were proposed in this region of nuclei promising further success. The role of 3-body residual interactions in nuclear chains in a single j-shell is discussed within the shell model [94]. Beyond the standard shell-model approach, the 3-body interaction was considered in calculations of the energies of excited states in $N = 50$ isotones [95], which caused a significant improvement in reproducing experimental values. Furthermore, nuclear flied theory group investigated Sn isotopic chain using particle-vibration coupling [96]. The quadrupole-vibrational excitations in even–even Cd isotopes was revisited by the mean-field interacting boson model [97].

As already indicated in the introduction the ab initio methods are recently possible for this region of nuclei. The prediction of energies of excited states of nuclei in vicinity of ^{100}Sn were very recently presented based on the particle-hole effective interaction derived from shell model couple cluster method [98].

4. Results

The results presented in this paper are narrowed to the three aspects of the structure of ^{100}Sn with an idea of demonstrating the role of like-nucleon vs. proton-neutron coupling in the $g_{9/2}$ shell (see Figure 1). First, the evolution of excited states was examined along the $N = 50$ line describing seniority in a $g_{9/2}{}^{n}$ and simple level coupling $g_{9/2}p_{1/2}$. Additionally, a JUN45 calculation and, even larger model spaces when available, are presented. Second, the $N = Z$ line is analyzed below ^{100}Sn where the shape change is expected along the $g_{9/2}{}^{n}$ orbital configuration. The recent developments in nuclear structure above $N = 50$ is summarized in the last subsection.

4.1. Nuclei below ^{100}Sn, $A \leq 100$

4.1.1. Even-Even $N = 50$ Isotones of the $g_{9/2}$ Shell

The seniority quantum number υ, which counts the number of unpaired nucleons for protons and neutrons occupying the same shell-model orbital, is very useful when

discussing the structure based on high-spin orbitals. Just below ^{100}Sn, isotopes with even Z form a long chain of a seniority isomers, which exhibit observable decays as the $g_{9/2}$ is well isolated from other high spin orbitals. A direct consequence of the short-range nature of the nucleon-nucleon interaction is the conservation of the seniority υ in any n-particle configuration j^n of like particles [99].

As the mixing of states with different seniority is expected to be small, several symmetries are imposed [24,100] (and references therein), of which the constant excitation energies within the shell and symmetry against the mid shell of $B(E2)$ values for transitions with non-changing seniority, are addressed in this Section. In Figure 3 the experimental excitation energies for the 2^+–8^+ levels, as well as 5^- are shown with the differently-colored symbols for each spin value. The lowering of the excitation energy seen for the states with even spin values is understood mostly by the increased binding of the 0^+ ground-state when removing protons from ^{100}Sn. This effect is caused by the contribution of lower shell orbitals such as $p_{3/2}$ and $f_{5/2}$, becoming closer to the Fermi level.

Most of the shell-model calculations, presented for $N = 50$ isotones, can reproduce level energies relatively well, with less accuracy for the 6^+ and 8^+ states. For the GF shell-model calculation (shown with continuous lines in Figure 3), the agreement is very good (note the expanded energy scale) in the lower shell e.g., for ^{92}Mo, which is trivial as it was used to fit the two-body matrix elements (TBME) and therefore effectively includes the contribution of lower shells. It is also understandable that there is a trend of increased level deviation of the $g_{9/2}{}^n$ coupling towards ^{100}Sn.

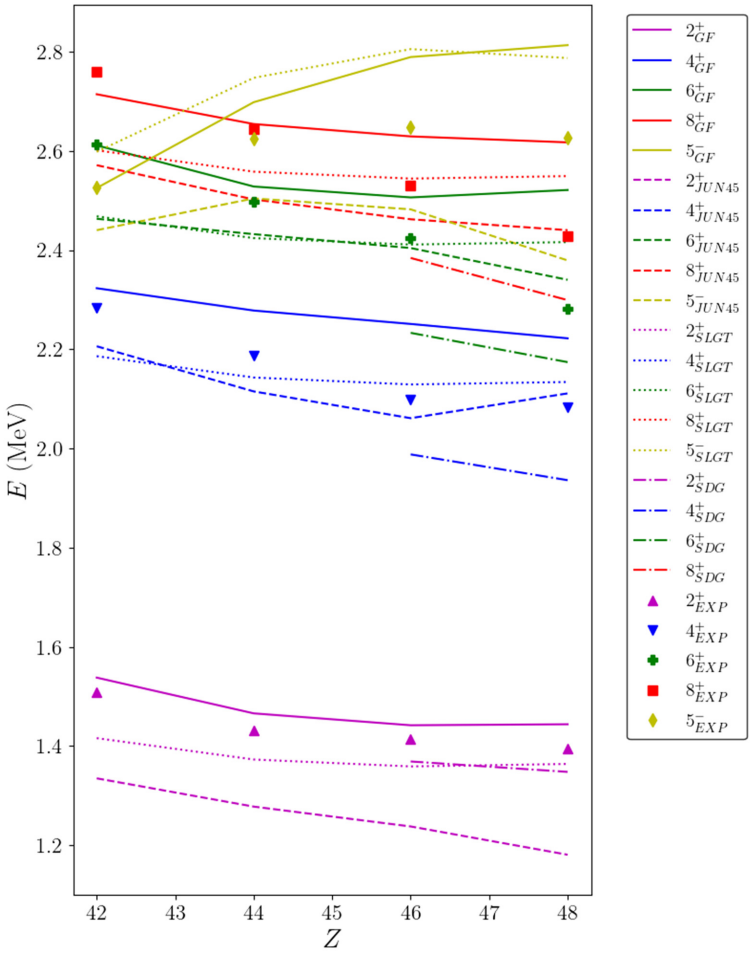

Figure 3. Systematics of the level energies in the N (number of neutrons) = 50 isotonic chain, for even-Z (atomic number) nuclei. Experimental data shown with colored symbols are taken from [101].

The energy of the 5^- state in ^{98}Cd is taken from [102]. The lines shown in corresponding colors represent theoretical level energies. Calculations were done with the NuShellX code [87] using empirical interaction GF [85], SLGT [86] in the $\pi(g_{9/2}p_{1/2})$ and realistic effective interaction JUN45 [78] in the $\pi(f_{5/2},p_{3/2},p_{1/2},g_{9/2})$ and SDG in $\pi\upsilon(g_{9/2},d_{5/2},g_{7/2},s_{1/2},d_{3/2})$ model spaces [92]. The values of single-particle level energies were adopted from [1]. A pure $\pi {g_{9/2}}^{n}$ configuration explains the levels 2^+–8^+. The 5^- states are obtained from the $\pi {p_{1/2}}^{-1} {g_{9/2}}^{n+1}$ coupling. The "EXP" denotes experimental values.

To note is that the newly-observed 5^- state in ^{98}Cd [102] completes its systematics in those nuclei build of coupling $\pi {p_{1/2}}^{-1} {g_{9/2}}^{n+1}$ and resembles the trend of increasing deviation towards the full shell. The discrepancy of the calculated 5^- and 8^+ states from the experimental values are almost identical, while their crossing is reproduced almost perfectly at ^{94}Ru. For the calculations using SLGT interaction (dotted lines in Figure 3), instead, the absolute values of energies are improving with increasing Z towards ^{96}Pd and worsen again for ^{98}Cd (except the 2^+ state).

The energy trend of 5^- states along the shell is not reproduced, similarly as for GF interaction. While for the low-spin states the JUN45 [78] spectrum is compressed, the 6^+ and 8^+ are rather well reproduced, improving further towards the end of the shell (dashed line). The 5^- state is missed by about 200 keV, which indicates the $p_{1/2}$ single particle evolution correction needed for those isotopes.

The SDG spectrum is generally contracted, caused by the inclusion of core excitations, but it reproduces consistently the slope of the line between ^{96}Pd and ^{98}Cd for which the calculation is available [92]. Moreover, the second 4^+ state (not shown in the figure for clarity) is predicted only 250 keV higher than the first one, which is approximately at the same energy as the first 6^+ state. In contrast, the second 6^+ state is predicted about 400 keV above the first one, which is considerably higher than the 8^+ state [92].

More relevant for the wave functions, however, is the comparison of experimental reduced transition probabilities, *B(E2)* values in $N = 50$ isotones with the calculated values. In that case, all calculations including the GF calculations, presented here, can reproduce the data rather well for the 6^+ and 8^+ states as their wave functions are mostly not affected by other configurations; see [1,100] and references therein. The $B(E2)$ for transition from the 6^+ state in ^{98}Cd became recently available and the accuracy of that from 8^+ state was improved [56]. The lower lying yrast states, however, caused an extended discussion in recent years on seniority conservation and seniority mixing in the $g_{9/2}$ orbital; see [1,100,103] and references therein.

Particularly for the nonaligned 4^+ systematics in the mid shell, of which two different seniority states are predicted in close vicinity, evidence is discussed [100] for seniority breakdown due to neutron excitations across the $N = 50$ shell gap. There, the clear advantage of LSSM calculation with core excitations included is evident. An extension of the experimental data to lower Z for $N = 50$ isotones will be soon available [104,105] and therefore the discussion on this topic is not extended in this work.

4.1.2. $N = Z$ Chain from ^{100}Sn to ^{80}Zr

The region of the heaviest and bound $N = Z$ nuclei is below ^{100}Sn. This fact makes it particularly attractive for studies of proton-neutron correlations and their dependance on the spin of the nucleus. Already decades ago theoretical calculations predicted the existence of $I^\pi = 16^+$ and $I^\pi = 25/2^+$ high-spin isomers in ^{96,97}Cd, respectively. Only much later, technical advances allowed the confirmation of these isomers experimentally [22,106].

Early shell-model studies employing empirical interactions in the $\pi\nu(p_{1/2}, g_{9/2})$ model space were reviewed in Ref. [1]. Realistic interactions with LSSM calculations were presented for the full $\pi\nu(f_{5/2},p_{3/2},p_{1/2},g_{9/2})$ model space [78,79,107–109] as well as for the upper $\pi\nu(gds)$ shell using the SDG interaction [110]. The strength of the $\pi\nu$ interaction in the $\pi\nu g_{9/2}$ orbits manifests itself best in the strongly-binding $T = 0$, $I^\pi = 9^+$ TBME, which is comparable in strength with the "normal", $T = 1$ pairing mode [85,86]. With the identification of excited states in ^{92}Pd [23], the role of the $\pi\nu g_{9/2}$ pairs with maximum spin of $I^\pi = 9^+$

in the $N = Z$ nuclei ^{96}Cd, ^{94}Ag and ^{92}Pd has been investigated in a series of multi-step shell model and IBM studies with respect to the "fully aligned" 9^+ -TBME [24,111–114].

The experimental yrast states for the even–even $N = Z$ nuclei in the $g_{9/2}$ shell are shown with colored symbols in Figure 4. For the lower mass $N = Z$ even–even nuclei the level structure implies an onset of deformation. The spectrum of ^{88}Ru [42] exhibits a rotational band similar to the known states of ^{84}Mo [115]. This could intuitively understood, similarly to the $N = 50$ chain, as even stronger influence by the lower shell *fp*-shell therefore driving deformation. However, recent developments in the calculation power could disprove this hypothesis, as shown below.

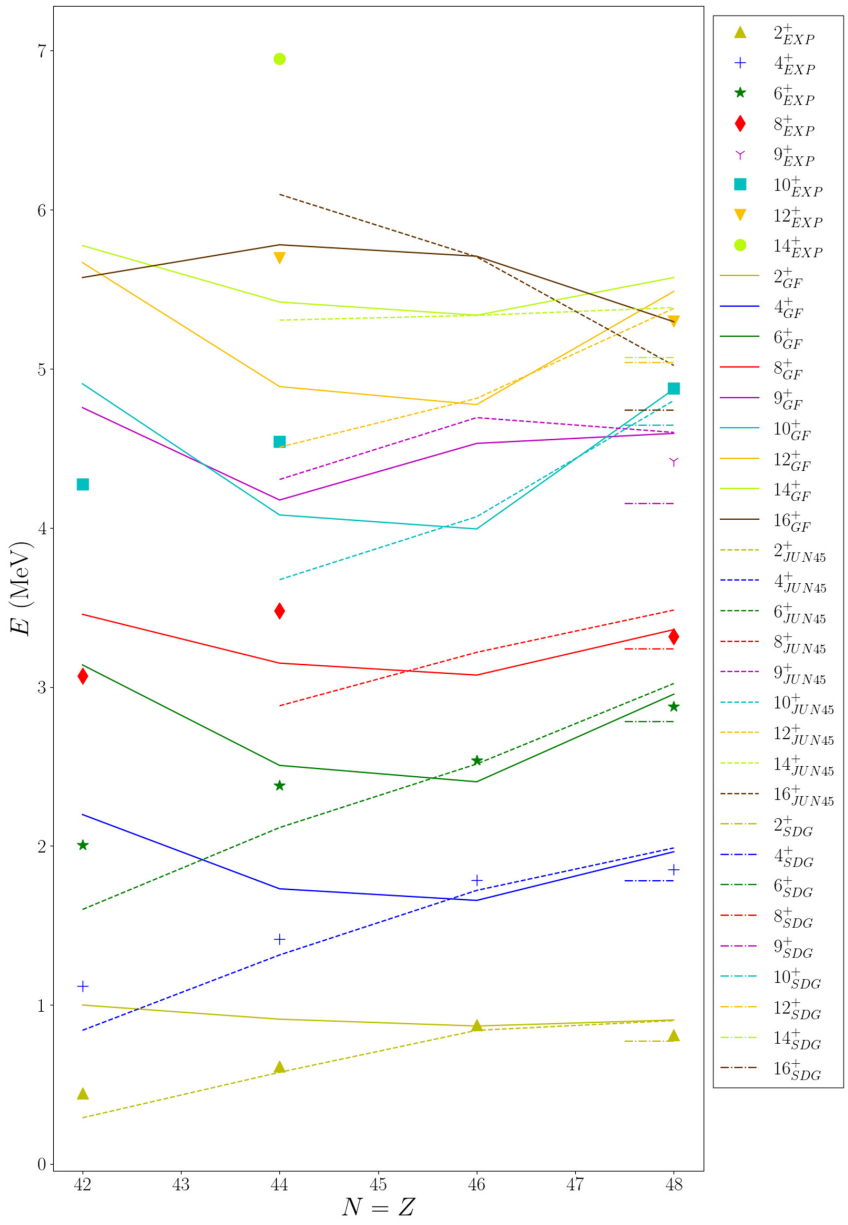

Figure 4. Excitation energies of the even–even $N = Z$ nuclei in the $g_{9/2}$ shell with A (atomic mass number) = 84–96 for spins $I^\pi = 2^+$–16^+. The spins of excited states in all isotopes are assigned tentatively [101]. Experimental energies are given with colored symbols distinguished by their spin values. Shell-model calculations are shown with solid lines with different colors for each spin for the GF [85] calculation, dashed line for the JUN45 calculation [78,107] and present work for the higher-spin states and colored and short dashed-dotted colored lines for SDG [110] calculation for ^{96}Cd.

Various shell-model approaches in different model spaces have been reported for this region. The calculation presented with solid colored lines is GF [85], which includes all yrast spins states up to the 16^+ for all the $N = Z$ nuclei in $g_{9/2}$ shell nuclei and in particular an isomeric trap, known to exist experimentally in ^{96}Cd [110]. Calculation using JUN45 interactions [78] are shown with dashed lines whenever possible for the computer power available within this work or in the literature [78,107].

The LSSM SDG [22] approach with up to $5p5h$ excitations (t = 5) across the Z, $N = 50$ closed shell are available only for ^{96}Cd up to high spins and is shown with short, colored dashed-dotted lines. A consistent description for all the calculations is obtained in the upper $g_{9/2}$ shell, as shown for ^{96}Cd. However, towards the mid shell, the $N = Z$ results are hampered by severe truncation. The advantage of including a larger model space, particularly the lower-lying orbitals, is evident. Nevertheless, with increasing spin the lower-shell nuclei follow very different trend than the predicted one.

According to the GF calculation presented in Figure 4, the spin trap at $I^\pi = 16^+$ in ^{84}Mo will stay yrast even if the spherical 0^+ state in the small model space of GF calculation is shifted by ~2 MeV up in energy with respect to the known deformed ground state and the rotational band member energies extrapolated with a constant moment of inertia to higher spins [115].

However, a common conclusion of various shell model approaches with $Z \geq 40$, $N = Z$ nuclei is the quest to include excitations across the Z, $N = 50$ shell closure [79,116–119] in order to attempt the description of the deformation. ^{84}Mo marks the transitional region where the shape-driving role of the $r3g$ space is replaced/enhanced by the gds space [79]. The spectra of ^{96}Cd is a benchmark for both model spaces and yield similar results. In addition, the ^{84}Mo spectrum was calculated with the help of the nucleon-pair approximation method [120], which also could be expanded to higher spins and other $N = Z$ nuclei in the $g_{9/2}$ shell in the future.

Recently, a new approach was proposed in the mean field [95], where within a simple SO(8) pairing model, it was shown that the symmetry-projected condensates of mixed isovector and isoscalar pairs very accurately describe properties of the exact solutions, including the coexistence of the isovector and isoscalar pairing. Lack of symmetry restoration thus explains the limited success in describing such a coexistence in the standard mean-field approaches to date. It was concluded that the future work investigating properties of the proton-neutron nuclear pairing can be carried out within the variation-after-projection approach to mean-field pairing methods.

4.2. Nuclei with N > 50

The Sn isotopes represent the longest chain of semi-magic nuclei, which makes them attractive for studies of shell-structure evolution as a function of the number of neutrons and how it can be related to collective as well to single-particle effects. The known, almost constant excitation energy of the first 2^+ state in the Sn isotopic chain has been a textbook example of the seniority scheme for a long time.

A sensitive probe for correlations of this kind is to measure transition probabilities for first excited selected states, which will manifest the configuration content of those states. With this approach the results of LSSM calculations based on microscopically-derived interactions can be tested through direct comparison with experiment. This approached was recognized with the availability of radioactive beams, and new measurements or new theory values have been seen frequently in recent years. A recent update on 6^+ states in Sn isotopes is reported in [61] for the 6^+ state lifetime and effective charge analysis. The energy of the second 2^+ state in ^{102}Sn was recently claimed in Ref. [121].

However, the main focus in the studies of Sn isotopes is on the first 2^+ states since the first measurement of radioactive isotopes 16 years ago [122], and the last ones being the theoretical study of Togashi et al. [77] and experimental study of Siciliano et al. [29]. The study of Togashi et al., represents the first approach in which it is possible to reproduce remarkably well the whole Sn chain (shown in Figure 2 of [77]) in same calculation.

The method used for this unified description of the detailed nuclear structure is Monte Carlo Shell Model including isospin conserving interaction calculation of the *gds* HO shell as well as the lower part of the neighboring HO shells [77] (and reference therein). An alternative calculation with a small modification is shown by the authors as to give an Ansatz to the experimentalists for a more precise experimental answer to the values in the mid-shell.

Within the generalized seniority scheme this mid-shell valley would be interpreted as changing single-particle orbitals filled along the Sn chain (see also [123]). In Figure 3 of [77] the authors describe the complex wave functions including core excitation (and deformation) for the 2^+ as well as the 4^+ states in Sn isotopes towards the mid shell modified by the quadrupole component of the proton-neutron interaction, which was first postulated in [124] by the LSSM analysis for the 2^+ states. The quadrupole collectivity was also predicted in Ref. [12].

The results, presented in Figure 3 by Siciliano et al. [29], show an overview of experimental knowledge on $B(E2{:}2^+ \rightarrow 0^+)$ for the full Sn isotopic chain based on intense efforts of many laboratories and experimental groups. References [122,124–144] represent a complete up-to-date list. The usage of general Doppler methods, such as the Doppler shift attenuation (DSAM) and the recoil distance Doppler shift methods (RDDS) to measure the lifetimes and to extract the $B(E2)$ values, were hampered until recently by the existence of higher-lying isomeric states.

Indeed, the authors of Ref. [29] managed to overcome the problem by using multi-nucleon transfer reactions and adjusting the excitation energy of the final product such that the 6^+ isomer feeding was minimized allowing for RDDS measurements. Moreover, the experimentalists harvested the first information on the lifetimes of 4^+ states, which opened up the systematics of $B(E2{:}4^+ \rightarrow 2^+)$ states below $N = 60$. This pioneering experimental work was accompanied by LSSM calculations, which could well reproduce experimental data using the new realistic effective interaction in the *gds* model space with a proper monopole treatment.

Another calculation indicating for the first time the double-hump shape associated to the quadrupole dominance, as shown in Ref. [77], refer to the importance of further investigations of the 4^+ states, where pairing effects related to single particle energies dominate instead. The new findings, together with the recent theory calculation [145] request for further experimental and theoretical effort in this direction.

The systematics of the reduced transition probabilities, the $B(E2{:}2^+ \rightarrow 0^+)$ values, is expected to be completed soon with the inclusion of the ^{102}Sn value [146]. The review dedicated to nuclear collectivity is in preparation [147], where updated figure will be presented.

Alternatively, the collective properties of ^{100}Sn can be approached again by studying nuclei with slightly lower Z. Several dedicated attempts for such experiments were undertaken at ISOLDE and NSCL. In particular, light Cd isotopes were addressed already in earlier days and Coulomb excitation transition probabilities and quadrupole moments were extracted up to ^{102}Cd [70]. The latest update on this can be found in [148], where $B(E2{:}4^+ \rightarrow 2^+)$ values were also measured, and the accompanying theory work, which attempted to explain particular conditions for collectivity in light Cd isotopes [70].

The beyond-mean-field calculations, presented in Ref. [148], reproduce the cadmium systematics, but also predict rotational structures for all of the $Z = 48$ isotopes, breaking the common view of the textbook example of vibrational nuclei. In addition, there (and in Ref. [85] therein), $Z = 48$ isotopes are predicted to be semi-magic deformed nuclei. The lightest Cd isotope for which $B(E2{:}2^+ \rightarrow 0^+)$ value measurement was attempted thus far is ^{100}Cd [70].

5. Summary and Outlook

Recent years have shown a great deal of interest from experimental and theoretical groups from all over the globe dedicated to investigations of the ^{100}Sn region. This materialized in many publications (referred to here and with more to come) in the last decade, as well as active and waiting proposals and, presently, a large amount of as-yet unevaluated data. The primary reason for the particular excitement is the relevance of this region for understanding the nuclear force in general and various specific aspects that can be uniquely studied in this region of the heaviest doubly-magic $N = Z$ nucleus.

To further encourage a steady level of development and the need for new data of key nuclei and particular states, two examples are mentioned here. The first one is the search for excited states in ^{100}Sn, which could be determined from the decay of the predicted isomeric 6^+ state [93] (and references therein). The second is excited states in ^{98}Sn (predictions presented in Figure 5), a mirror nucleus of ^{98}Cd [149]. Those two nuclei likely constitute the heaviest possibly bound mirror pairs of all nuclei.

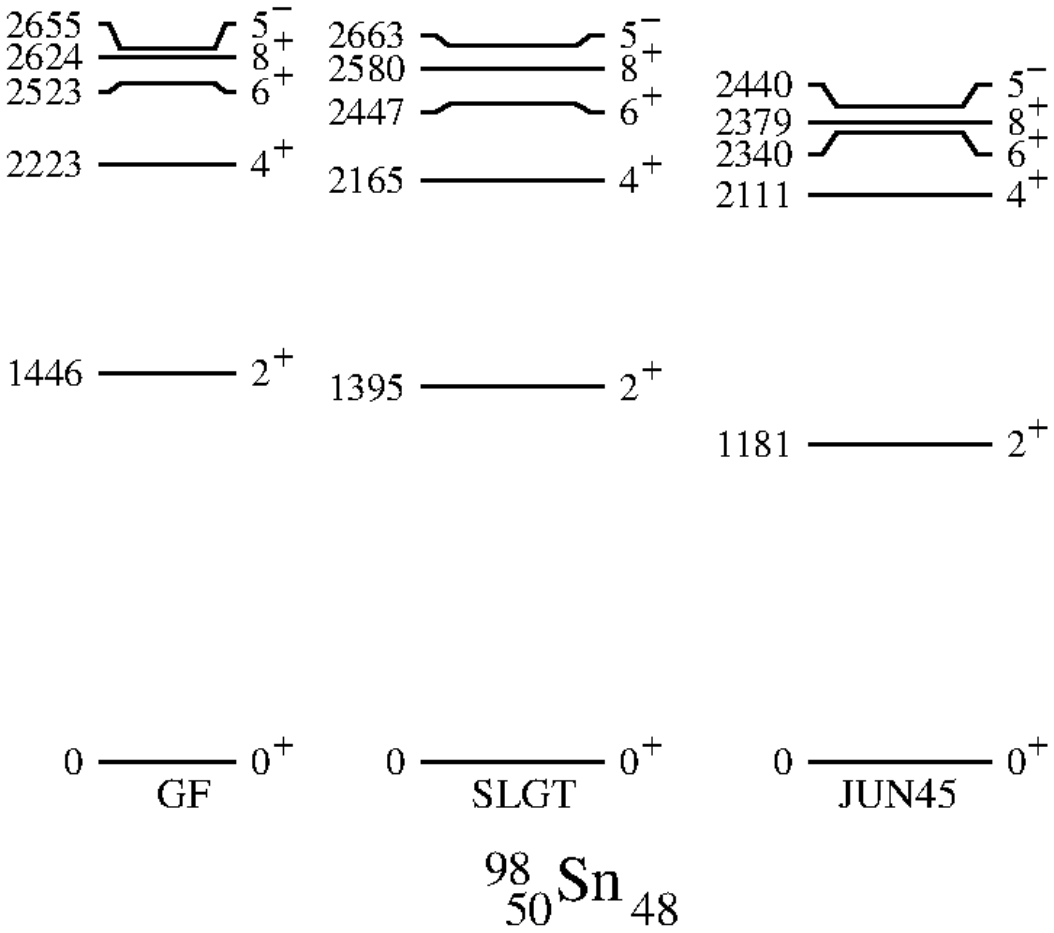

Figure 5. Predictions of the ^{98}Sn excited states according to the available interactions. All of them suggest an 8^+ isomeric state as the one known in the mirror nucleus ^{98}Cd [149]. The JUN45 spectrum is identical to that one of ^{98}Cd because of the isospin symmetry of this interaction.

Funding: This research received no external funding.

Data Availability Statement: No new data were created or analyzed in this study. Data sharing is not applicable to this article.

Acknowledgments: Hubert Grawe is gratefully acknowledged post mortem for his mentoring until his very last days. Without him, this paper would not be possible. Andrey Blazhev, Piet Van Isacker, Frédéric Nowacki and Taka Otsuka are acknowledged for useful discussions and support. Kathrin Wimmer is acknowledged for introducing the author to the basics of Python libraries as well as for running calculations with JUN45 interaction for high spin states in $N = Z$ nuclei on a larger computer than available for the author. Zsolt Podolyák and Helena May Albers are acknowledged for valuable comments and proofreading of this article.

Conflicts of Interest: The author declares no conflict of interest.

References

1. Faestermann, T.; Górska, M.; Grawe, H. The structure of ^{100}Sn and neighbouring nuclei. *Prog. Part. Nucl. Phys.* **2013**, *69*, 85–130. [CrossRef]
2. Dobaczewski, J.; Nazarewicz, W. Limits of proton stability near ^{100}Sn. *Phys. Rev. C* **1995**, *51*, R1070–R1073. [CrossRef] [PubMed]
3. Neufcourt, L.; Cao, Y.; Giuliani, S.; Nazarewicz, W.; Olsen, E.; Tarasov, O.B. Beyond the proton drip line: Bayesian analysis of proton-emitting nuclei. *Phys. Rev. C* **2020**, *101*, 014319. [CrossRef]
4. Arthuis, P.; Barbieri, C.; Vorabbi, M.; Finelli, P. Ab Initio Computation of Charge Densities for Sn and Xe Isotopes. *Phys. Rev. Lett.* **2020**, *125*, 182501. [CrossRef] [PubMed]
5. Reponen, M.; de Groote, R.P.; Al Ayoubi, L.; Beliuskina, O.; Bissell, M.L.; Campbell, P.; Cañete, L.; Cheal, B.; Chrysalidis, K.; Delafosse, C.; et al. Evidence of a sudden increase in the nuclear size of proton-rich silver-96. *Nat. Commun.* **2021**, *12*, 4596. [CrossRef] [PubMed]
6. Ferrer, R.; Bree, N.; Cocolios, T.E.; Darby, I.; De Witte, H.; Dexters, W.; Diriken, J.; Elseviers, J.; Franchoo, S.; Huyse, M.; et al. In-gas-cell laser ionization spectroscopy in the vicinity of ^{100}Sn: Magnetic moments and mean-square charge radii of N = 50–54 Ag. *Phys. Lett. B* **2014**, *728*, 191–197. [CrossRef]
7. Brown, B. The nuclear shell model towards the drip lines. *Prog. Part. Nucl. Phys.* **2001**, *47*, 517–599. [CrossRef]
8. Brown, B.A.; Rykaczewski, K. Gamow-Teller strength in the region of ^{100}Sn. *Phys. Rev. C* **1994**, *50*, R2270–R2273. [CrossRef]
9. Hinke, C.B.; Böhmer, M.; Boutachkov, P.; Faestermann, T.; Geissel, H.; Gerl, J.; Gernhäuser, R.; Górska, M.; Gottardo, A.; Grawe, H.; et al. Superallowed Gamow–Teller decay of the doubly magic nucleus ^{100}Sn. *Nature* **2012**, *486*, 341–345. [CrossRef]
10. Lubos, D.; Park, J.; Faestermann, T.; Gernhäuser, R.; Krücken, R.; Lewitowicz, M.; Nishimura, S.; Sakurai, H.; Ahn, D.S.; Baba, H.; et al. Improved Value for the Gamow-Teller strength of the ^{100}Sn beta decay. *Phys. Rev. Lett.* **2019**, *122*, 222502. [CrossRef]
11. Konieczka, M.; Satuła, W.; Kortelainen, M. Gamow-Teller response in the configuration space of a density-functional-theory–rooted no-core configuration-interaction model. *Phys. Rev. C* **2018**, *97*, 034310. [CrossRef]
12. Morris, T.D.; Simonis, J.; Stroberg, S.R.; Stumpf, C.; Hagen, G.; Holt, J.D.; Jansen, G.R.; Papenbrock, T.; Roth, R.; Schwenk, A. Structure of the Lightest Tin Isotopes. *Phys. Rev. Lett.* **2018**, *120*, 152503. [CrossRef]
13. Gysbers, P.; Hagen, G.; Holt, J.D.; Jansen, G.R.; Morris, T.; Navrátil, P.; Papenbrock, T.; Quaglioni, S.; Schwenk, A.; Stroberg, S.R.; et al. Discrepancy between experimental and theoretical β-decay rates resolved from first principles. *Nat. Phys.* **2019**, *15*, 428–431. [CrossRef]
14. Mougeot, M.; Atanasov, D.; Karthein, J.; Wolf, R.N.; Ascher, P.; Blaum, K.; Chrysalidis, K.; Hagen, G.; Holt, J.D.; Huang, W.J.; et al. Mass measurements of 99–101In challenge ab initio nuclear theory of the nuclide ^{100}Sn. *Nat. Phys.* **2021**, *17*, 1099–1103. [CrossRef]
15. Hornung, C.; Amanbayev, D.; Dedes, I.; Kripko-Koncz, G.; Miskun, I.; Shimizu, N.; Andrés, S.A.S.; Bergmann, J.; Dickel, T.; Dudek, J.; et al. Isomer studies in the vicinity of the doubly-magic nucleus ^{100}Sn: Observation of a new low-lying isomeric state in ^{97}Ag. *Phys. Lett. B* **2020**, *802*, 135200. [CrossRef]
16. Yang, S.; Xu, C.; Röpke, G.; Schuck, P.; Ren, Z.; Funaki, Y.; Horiuchi, H.; Tohsaki, A.; Yamada, T.; Zhou, B. α decay to a doubly magic core in the quartetting wave function approach. *Phys. Rev. C* **2020**, *101*, 024316. [CrossRef]
17. Clark, R.M.; Macchiavelli, A.O.; Crawford, H.L.; Fallon, P.; Rudolph, D.; Såmark-Roth, A.; Campbell, C.M.; Cromaz, M.; Morse, C.; Santamaria, C. Enhancement of α-particle formation near ^{100}Sn. *Phys. Rev. C* **2020**, *101*, 034313. [CrossRef]
18. Muir, D.; Pastore, A.; Dobaczewski, J.; Barton, C. Bootstrap technique to study correlation between neutron skin thickness and the slope of symmetry energy in atomic nuclei. *Acta Phys. Pol. B* **2018**, *49*, 359. [CrossRef]
19. Blazhev, A.; Górska, M.; Grawe, H.; Nyberg, J.; Palacz, M.; Caurier, E.; Dorvaux, O.; Gadea, A.; Nowacki, F.; Andreoiu, C.; et al. Observation of a core-excited *E4* isomer in ^{98}Cd. *Phys. Rev. C* **2004**, *69*, 064304. [CrossRef]

20. Blazhev, A.; Braun, N.; Grawe, H.; Boutachkov, P.; Singh, B.S.N.; Brock, T.; Liu, Z.; Wadsworth, R.; Gorska, M.; Jolie, J.; et al. High-energy excited states in98Cd. *J. Phys. Conf. Ser.* **2010**, *205*, 012035. [CrossRef]
21. Boutachkov, P.; Górska, M.; Grawe, H.; Blazhev, A.; Braun, N.; Brock, T.S.; Liu, Z.; Singh, B.S.N.; Wadsworth, R.; Pietri, S.; et al. High-spin isomers in ^{96}Ag: Excitations across the Z = 38 and Z = 50, N = 50 closed shells. *Phys. Rev. C* **2011**, *84*, 044311. [CrossRef]
22. Davies, P.J.; Park, J.; Grawe, H.; Wadsworth, R.; Gernhäuser, R.; Krücken, R.; Nowacki, F.; Ahn, D.S.; Ameil, F.; Baba, H.; et al. Toward the limit of nuclear binding on the $N = Z$ line: Spectroscopy of ^{96}Cd. *Phys. Rev. C* **2019**, *99*, 021302. [CrossRef]
23. Cederwall, B.; Moradi, F.G.; Bäck, T.; Johnson, A.; Blomqvist, J.; Clement, E.; de France, G.; Wadsworth, R.; Andgren, K.; Lagergren, K.; et al. Evidence for a spin-aligned neutron–proton paired phase from the level structure of ^{92}Pd. *Nature* **2010**, *469*, 68–71. [CrossRef] [PubMed]
24. Zamick, L.; Escuderos, A. Single *j*-shell studies of cross-conjugate nuclei and isomerism: $(2j - 1)$ rule. *Nucl. Phys. A* **2012**, *889*, 8–17. [CrossRef]
25. Goutte, H.; Navin, A. Microscopes for the physics at the femtoscale: GANIL-SPIRAL2. *Nucl. Phys. News* **2021**, *31*, 5–12. [CrossRef]
26. Nuclear Physics Facilities—Department of Physics. Available online: https://www.jyu.fi/en/frontpage (accessed on 1 August 2021).
27. Argonne Tandem Linac Accelerator System—Argonne National Laboratory. Available online: https://www.anl.gov/ (accessed on 1 August 2021).
28. Home INFN Legnaro—National Institute for Nuclear Physics. Available online: https://www.lnl.infn.it/en/welcome-on-the-site-of-the-national-laboratories-of-legnaro/ (accessed on 1 August 2021).
29. Siciliano, M.; Valiente-Dobón, J.; Goasduff, A.; Nowacki, F.; Zuker, A.; Bazzacco, D.; Lopez-Martens, A.; Clément, E.; Benzoni, G.; Braunroth, T.; et al. Pairing-quadrupole interplay in the neutron-deficient tin nuclei: First lifetime measurements of low-lying states in ^{106,108}Sn. *Phys. Lett. B* **2020**, *806*, 135474. [CrossRef]
30. Akkoyun, S.; Algora, A.; Alikhani, B.; Ameil, F.; de Angelis, G.; Arnold, L.; Astier, A.; Ataç, A.; Aubert, Y.; Aufranc, C.; et al. AGATA—Advanced GAmma Tracking Array. *Nucl. Instr. Meth. A* **2012**, *668*, 26. [CrossRef]
31. Clément, E.; Michelagnoli, C.; de France, G.; Li, H.J.; Lemasson, A.; Barthe Dejean, C.; Beuzard, M.; Bougault, P.; Cacitti, J.; Foucher, J.-L.; et al. Conceptual design of the AGATA π1 array at GANIL. *Nucl. Instr. Meth. A* **2017**, *855*, 1. [CrossRef]
32. Scheurer, J.; Aiche, M.; Aleonard, M.M.; Barreau, G.; Bourgine, F.; Boivin, D.; Cabaussel, D.; Chemin, J.F.; Doan, T.P.; Goudour, J.P.; et al. Improvements in the in-beam y-ray spectroscopy provided by an ancillary detector coupled to a Ge y-spectrometer: The Diamant-Eurogam II example. *Nucl. Instr. Meth. A* **1997**, *385*, 501. [CrossRef]
33. Gál, J.; Hegyesi, G.; Molnár, J.; Nyakó, B.; Kalinka, G.; Scheurer, J.; Aléonard, M.; Chemin, J.; Pedroza, J.; Juhász, K.; et al. The VXI electronics of the DIAMANT particle detector array. *Nucl. Instrum. Methods Phys. Res. Sect. A* **2004**, *516*, 502–510. [CrossRef]
34. Hüyük, T.; Di Nitto, A.; Jaworski, G.; Gadea, A.; Valiente-Dobón, J.J.; Nyberg, J.; Palacz, M.; Söderström, P.-A.; Aliaga-Varea, R.J.; De Angelis, G.; et al. Conceptual design of the early implementation of the NEutron Detector Array (NEDA) with AGATA. *Eur. Phys. J. A* **2016**, *52*, 55. [CrossRef]
35. Valiente-Dobón, J.J.; Jaworski, G.; Goasduff, A.; Egea, F.J.; Modamio, V.; Hüyük, T.; Triossi, A.; Jastrząb, M.; Söderström, P.A.; Di Nitto, A.; et al. NEDA—NEutron Detector Array. *Nucl. Instr. Meth. A* **2019**, *927*, 81. [CrossRef]
36. Pullanhiotan, S.; Chatterjee, A.; Jacquot, B.; Navin, A.; Rejmund, M. Improvement in the reconstruction method for VAMOS spectrometer. *Nucl. Instrum. Methods Phys. Res. Sect. B* **2008**, *266*, 4148–4152. [CrossRef]
37. Rejmund, M.; Lecornu, B.; Navin, A.; Schmitt, C.; Damoy, S.; Delaune, O.; Enguerrand, J.; Fremont, G.; Gangnant, P.; Gaudefroy, L.; et al. Performance of the improved larger acceptance spectrometer: VAMOS++. *Nucl. Instrum. Methods Phys. Res. Sect. A* **2011**, *646*, 184–191. [CrossRef]
38. Vandebrouck, M.; Lemasson, A.; Rejmund, M.; Fremont, G.; Pancin, J.; Navin, A.; Michelagnoli, C.; Goupil, J.; Spitaels, C.; Jacquot, B. Dual Position Sensitive MWPC for tracking reaction products at VAMOS++. *Nucl. Instrum. Methods Phys. Res. Sect. A* **2016**, *812*, 112–117. [CrossRef]
39. Mass Analysing Recoil Apparatus (MARA)—Department of Physics. Available online: https://www.jyu.fi/science/en/physics/research/infrastructures/accelerator-laboratory/nuclear-physics-facilities/recoil-separators/mara-mass-analysing-recoil-apparatus (accessed on 1 November 2021).
40. Davids, C.N.; Larson, J.D. The argonne fragment mass analyzer. *Nucl. Instr. Meth. B* **1989**, *40–41*, 1224. [CrossRef]
41. Kalandarov, S.A.; Adamian, G.G.; Antonenko, N.V.; Wieleczko, J.P. Production of the doubly magic nucleus ^{100}Sn in fusion and quasifission reactions via light particle and cluster emission channels. *Phys. Rev. C* **2014**, *90*, 024609. [CrossRef]
42. Cederwall, B.; Liu, X.; Aktas, Ö.; Ertoprak, A.; Zhang, W.; Qi, C.; Clément, E.; de France, G.; Ralet, D.; Gadea, A.; et al. Isospin properties of nuclear pair correlations from the level structure of the self-conjugate nucleus ^{88}Ru. *Phys. Rev. Lett.* **2020**, *124*, 062501. [CrossRef]
43. Auranen, K. Superallowed α decay to doubly magic ^{100}Sn. *Phys. Rev. Lett.* **2018**, *121*, 182501. [CrossRef]
44. Seweryniak, D.; Carpenter, M.P.; Gros, S.; Hecht, A.A.; Hoteling, N.; Janssens, R.V.F.; Khoo, T.L.; Lauritsen, T.; Lister, C.J.; Lotay, G.; et al. Single-neutron states in ^{101}Sn. *Phys. Rev. Lett.* **2007**, *99*, 022504. [CrossRef]

45. Xiao, Y.; Go, S.; Grzywacz, R.; Orlandi, R.; Andreyev, A.N.; Asai, M.; Bentley, M.A.; de Angelis, G.; Gross, C.J.; Hausladen, P.; et al. Search for α decay of ^{104}Te with a novel recoil-decay scintillation detector. *Phys. Rev. C* **2019**, *100*, 034315. [CrossRef]
46. Darby, I.G.; Grzywacz, R.K.; Batchelder, J.C.; Bingham, C.R.; Cartegni, L.; Gross, C.J.; Hjorth-Jensen, M.; Joss, D.T.; Liddick, S.N.; Nazarewicz, W.; et al. Orbital dependent nucleonic pairing in the lightest known Isotopes of Tin. *Phys. Rev. Lett.* **2010**, *105*, 162502. [CrossRef] [PubMed]
47. Erler, J.; Birge, N.; Kortelainen, M.; Nazarewicz, W.; Olsen, E.; Perhac, A.M.; Stoitsov, M. The limits of the nuclear landscape. *Nature* **2012**, *486*, 509–512. [CrossRef] [PubMed]
48. Kubo, T.; Kameda, D.; Suzuki, H.; Fukuda, N.; Takeda, H.; Yanagisawa, Y.; Ohtake, M.; Kusaka, K.; Yoshida, K.; Inabe, N.; et al. BigRIPS separator and ZeroDegree spectrometer at RIKEN RI Beam Factory. *Prog. Theor. Exp. Phys.* **2012**, *2012*, 03C003. [CrossRef]
49. RIKEN. Euroball-RIKEN Cluster Array (EURICA) Project Unveiled. Available online: https://www.riken.jp/en/news_pubs/news/2012/20120326_4/index.html (accessed on 1 August 2021).
50. Takeuchi, S.; Motobayashi, T.; Togano, Y.; Matsushita, M.; Aoi, N.; Demichi, K.; Hasegawa, H.; Murakami, H. DALI2: A NaI(Tl) detector array for measurements of γ-rays from fast nuclei. *Nucl. Instr. Meth. A* **2014**, *763*, 596. [CrossRef]
51. Čeliković, I.; Lewitowicz, M.; Gernhäuser, R.; Krücken, R.; Nishimura, S.; Sakurai, H.; Ahn, D.; Baba, H.; Blank, B.; Blazhev, A.; et al. New isotopes and proton emitters–Crossing the drip line in the vicinity of ^{100}Sn. *Phys. Rev. Lett.* **2016**, *116*, 162501. [CrossRef]
52. Park, J.; Krücken, R.; Lubos, D.; Gernhäuser, R.; Lewitowicz, M.; Nishimura, S.; Ahn, D.S.; Baba, H.; Blank, B.; Blazhev, A.; et al. New and comprehensive β- and βp-decay spectroscopy results in the vicinity of ^{100}Sn. *Phys. Rev. C* **2019**, *99*, 034313. [CrossRef]
53. Park, J.; Krücken, R.; Blazhev, A.; Lubos, D.; Gernhäuser, R.; Lewitowicz, M.; Nishimura, S.; Ahn, D.; Baba, H.; Blank, B.; et al. Spectroscopy of ^{99}Cd and ^{101}In from β decays of ^{99}In and ^{101}Sn. *Phys. Rev. C* **2020**, *102*, 014304. [CrossRef]
54. Davies, P.; Grawe, H.; Moschner, K.; Blazhev, A.; Wadsworth, R.; Boutachkov, P.; Ameil, F.; Yagi, A.; Baba, H.; Bäck, T.; et al. The role of core excitations in the structure and decay of the 16+ spin-gap isomer in ^{96}Cd. *Phys. Lett. B* **2017**, *767*, 474–479. [CrossRef]
55. Häfner, G.; Moschner, K.; Blazhev, A.; Boutachkov, P.; Davies, P.J.; Wadsworth, R.; Ameil, F.; Baba, H.; Bäck, T.; Dewald, M.; et al. Properties of γ-decaying isomers in the ^{100}Sn region populated in fragmentation of a ^{124}Xe beam. *Phys. Rev. C* **2019**, *100*, 024302. [CrossRef]
56. Park, J.; Krücken, R.; Lubos, D.; Gernhäuser, R.; Lewitowicz, M.; Nishimura, S.; Ahn, D.S.; Baba, H.; Blank, B.; Blazhev, A.; et al. Properties of γ -decaying isomers and isomeric ratios in the ^{100}Sn region. *Phys. Rev. C* **2017**, *96*, 044311. [CrossRef]
57. Doornenbal, P. In-beam gamma-ray spectrometer at the RIBF. *Prog. Theor. Exp. Phys.* **2012**, *2012*, 03C004. [CrossRef]
58. Loruso, G.; Becerril, A.D.; Amthor, A.M.; Baumann, T. β-delayed proton emission in the ^{100}Sn region. *Phys. Rev. C* **2012**, *86*, 014313. [CrossRef]
59. Cerizza, G.; Ayres, A.; Jones, K.L.; Grzywacz, R.; Bey, A.; Bingham, C.; Cartegni, L.; Miller, D.; Padgett, S.; Baugher, T.; et al. Structure of ^{107}Sn studied through single-neutron knockout reactions. *Phys. Rev. C* **2016**, *93*, 021601. [CrossRef]
60. Hamaker, A.; Leistenschneider, E.; Jain, R.; Bollen, G.; Giuliani, S.A.; Lund, K.; Nazarewicz, W.; Neufcourt, L.; Nicoloff, C.R.; Puentes, D.; et al. Precision mass measurement of lightweight self-conjugate nucleus 80Zr. *Nat. Phys.* **2021**, *17 1408*, 1–5. [CrossRef]
61. Grawe, H.; Straub, K.; Faestermann, T.; Górska, M.; Hinke, C.; Krücken, R.; Nowacki, F.; Böhmer, M.; Boutachkov, P.; Geissel, H.; et al. The (6+) isomer in ^{102}Sn revisited: Neutron and proton effective charges close to the double shell closure. *Phys. Lett. B* **2021**, *820*, 136591. [CrossRef]
62. Pietri, S.; Regan, P.H.; Podolyak, Z.; Rudolph, D.; Steer, S.; Garnsworthy, A.B.; Werner-Malento, E.; Hoischen, R.; Górska, M.; Gerl, J.; et al. Recent results in fragmentation isomer spectroscopy with rising. *Nucl. Instr. Met. B* **2007**, *261*, 1079. [CrossRef]
63. Geissel, G.; Armbruster, P.; Behr, K.H.; Brünle, A.; Burkard, K.; Chen, M.; Folger, H.; Franczak, B.; Keller, H.; Klepperet, O.; et al. The GSI projectile fragment separator (FRS): A versatile magnetic system for relativistic heavy ions. *Nucl. Instr. Meth. B* **1992**, *70*, 286. [CrossRef]
64. Mistry, A.K.; Albers, H.M.; Arıcı, T.; Banerjee, A.; Benzoni, G.; Cederwall, B.; Gerl, J.; Górska, M.; Hall, O.; Hubbard, N.; et al. The DESPEC setup for GSI and FAIR. *Nucl. Inst. Meth. B*, *in print*.
65. Technical Report for the Design, Construction and Commissioning of FATIMA, the FAst TIMing Array (2015). Available online: https://edms.cern.ch/document/1865981/1 (accessed on 1 August 2021).
66. Kester, O.; Sieber, T.; Emhofer, S.; Ames, F.; Reisinger, K.; Reiter, P.; Thirolf, P.; Lutter, R.; Habs, D.; Wolf, B.; et al. Accelerated radioactive beams from REX-ISOLDE. *Nucl. Instrum. Methods Phys. Res. Sect. B* **2002**, *204*, 20–30. [CrossRef]
67. Borge, M. Highlights of the ISOLDE facility and the HIE-ISOLDE project. *Nucl. Instrum. Methods Phys. Res. Sect. B* **2016**, *376*, 408–412. [CrossRef]

68. Eberth, J.; Pascovici, G.; Thomas, H.; Warr, N.; Weisshaar, D.; Habs, D.; Reiter, P.; Thirolf, P.; Schwalm, D.; Gund, C.; et al. MINIBALL A Ge detector array for radioactive ion beam facilities. *Prog. Part. Nucl. Phys.* **2001**, *46*, 389–398. [CrossRef]
69. Warr, N.; Van De Walle, J.; Albers, M.; Ames, F.; Bastin, B.; Bauer, C.; Bildstein, V.; Blazhev, A.; Bönig, S.; Bree, N.; et al. The Miniball spectrometer. *Eur. Phys. J. A* **2013**, *49*, 40. [CrossRef]
70. Ekström, A.; Cederkäll, J.; DiJulio, D.D.; Fahlander, C.; Hjorth-Jensen, M.; Blazhev, A.; Bruyneel, B.; Butler, P.A.; Davinson, T.; Eberth, J.; et al. Electric quadrupole moments of the 21+states in Cd100,102,104. *Phys. Rev. C* **2009**, *80*, 054302. [CrossRef]
71. Ekstrom, A.; Cederkall, J.; Fahlander, C.; Hjorth-Jensen, M.; Engeland, T.; Blazhev, A.; Butler, P.A.; Davinson, T.; Eberth, J.; Finke, F.; et al. Coulomb excitation of the odd-odd isotopes $^{106,\,108}$In. *Eur. Phys. J. A* **2010**, *44*, 355–361. [CrossRef]
72. DiJulio, D.D.; Cederkall, J.; Fahlander, C.; Ekstrom, A.; Hjorth-Jensen, M.; Albers, M.; Bildstein, V.; Blazhev, A.; Darby, I.; Davinson, T.; et al. Excitation strengths in ^{109}Sn: Single-neutron and collective excitations near ^{100}Sn. *Phys. Rev. C* **2012**, *86*, 031302. [CrossRef]
73. DiJulio, D.D.; Cederkall, J.; Fahlander, C.; Ekstrom, A.; Hjorth-Jensen, M.; Albers, M.; Bildstein, V.; Blazhev, A.; Darby, I.; Davinson, T.; et al. Coulomb excitation of ^{107}Sn. *Eur. Phys. J. A* **2012**, *48*, 105. [CrossRef]
74. DiJulio, D.; Cederkall, J.; Fahlander, C.; Ekström, A. Coulomb excitation of ^{107}In. *Phys. Rev. C* **2013**, *87*, 017301. [CrossRef]
75. Lunderberg, E.; Belarge, J.; Bender, P.; Bucher, B.; Cline, D.; Elman, B.; Gade, A.; Liddick, S.; Longfellow, B.; Prokop, C.; et al. JANUS—A setup for low-energy Coulomb excitation at ReA3. *Nucl. Instrum. Methods Phys. Res. Sect. A* **2018**, *885*, 30–37. [CrossRef]
76. Rhodes, D.; Brown, B.A.; Henderson, J.; Gade, A.; Ash, J.; Bender, P.C.; Elder, R.; Elman, B.; Grinder, M.; Hjorth-Jensen, M.; et al. Exploring the role of high-*j* configurations in collective observables through the Coulomb excitation of ^{106}Cd. *Phys. Rev. C* **2021**, *103*, L051301. [CrossRef]
77. Togashi, T.; Tsunoda, Y.; Otsuka, T.; Shimizu, N.; Honma, M. Novel shape evolution in Sn isotopes from magic numbers 50 to 82. *Phys. Rev. Lett.* **2018**, *121*, 062501. [CrossRef] [PubMed]
78. Honma, M.; Otsuka, T.; Mizusaki, T.; Hjorth-Jensen, M. New effective interaction for f_5pg_9-shell nuclei. *Phys. Rev. C* **2009**, *80*, 064323. [CrossRef]
79. Zuker, A.P.; Poves, A.; Nowacki, F.; Lenzi, S.M. Nilsson-SU3 self-consistency in heavy N = Z nuclei. *Phys. Rev. C* **2015**, *92*, 024320. [CrossRef]
80. Gargano, A.; Coraggio, L.; Covello, A.; Itaco, N. Investigating neutron-deficient tin isotopes via realistic shell-model calculations. *AIP Conf. Proc.* **2015**, *1681*, 020007.
81. Coraggio, L.; Gargano, A.; Itaco, N. Double-step truncation procedure for large-scale shell-model calculations. *Phys. Rev. C* **2016**, *93*, 064328. [CrossRef]
82. Zucker, A. Quadrupole dominance in the light Sn and in the Cd isotope. *Phys. Rev. C* **2021**, *103*, 024322. [CrossRef]
83. Coraggio, L.; Itaco, N. Perturbative approach to effective shell-model hamiltonians and operators. *Front. Phys.* **2020**, *8*, 345. [CrossRef]
84. Gargano, A.; Coraggio, L.; Itaco, N. Effectively-truncated large-scale shell-model calculations and nuclei around ^{100}Sn. *Phys. Scr.* **2017**, *92*, 094003. [CrossRef]
85. Gross, R.; Frenkel, A. Effective interaction of protons and neutrons in the $2p_{12}$-$1g_{92}$ subshells. *Nucl. Phys. A* **1976**, *267*, 85. [CrossRef]
86. Serduke, F.J.D.; Lawson, R.D.; Gloeckner, D.H. Shell-modelstudy of the N = 49 isotones. *Nucl. Phys. A* **1976**, *256*, 45. [CrossRef]
87. Brown, B.A.; Rae, W.D.M. The Shell-Model Code NuShellX@MSU. *Nucl. Data Sheets* **2014**, *120*, 115. [CrossRef]
88. Hjorth-Jensen, M.; Kuo, T.T.; Osnes, E. Realistic effective interactions for nuclear systems. *Phys. Rep.* **1995**, *261*, 125–270. [CrossRef]
89. Grawe, H.; Blazhev, A.; Górska, M. Correspondence Affiliation: GSI Darmstadt, Darmstadt, Germany. Empirically-modified realistic intereraction for the ^{100}Sn region. **2021**. to be published.
90. Yordanov, D.T.; Balabanski, D.L.; Bissell, M.L.; Blaum, K.; Blazhev, A.; Budinčević, I.; Frömmgen, N.; Geppert, C.; Grawe, H.; Hammen, M.; et al. Spins and electromagnetic moments of $^{101-109}$Cd. *Phys. Rev. C* **2018**, *98*, 011303. [CrossRef]
91. Coombes, B.J.; Stuchbery, A.E.; Blazhev, A.; Grawe, H.; Reed, M.W.; Akber, A.; Dowie, J.T.H.; Gerathy, M.S.M.; Gray, T.J.; Kibedi, T.; et al. Spectroscopy and excited-state g factors in weakly collective ^{111}Cd: Confronting collective and micro-scopic models. *Phys. Rev. C* **2019**, *100*, 024322. [CrossRef]
92. Nowacki, F. (Institut Pluridisciplinaire Hubert Curien, Strasbourg, France). Updated calculations with t=5. Private communication, 2021.
93. Arnswald, K.; Blazhev, A.; Nowacki, F.; Petkov, P.; Reiter, P.; Braunroth, T.; Dewald, A.; Droste, M.; Fransen, C.; Hirsch, R.; et al. Enhanced quadrupole collectivity in doubly-magic ^{56}Ni: Lifetime measurements of the 4_1^+ and 6_1^+ states. *Phys. Lett. B* **2021**, *820*, 136592. [CrossRef]

94. Derbali, E.; van Isacker, P.; Tellili, B.; Souga, C. Effective operators in a single-*j* orbital. *J. Phys. G Nucl. Part. Phys.* **2018**, *45*, 035102. [CrossRef]
95. Romero, A.; Dobaczewski, J.; Pastore, A. Symmetry restoration in the mean-field description of proton-neutron pairing. *Phys. Lett. B* **2019**, *795*, 177–182. [CrossRef]
96. Idini, A.; Potel, G.; Barranco, F.; Vigezzi, E.; Broglia, R.A. Interweaving of elementary modes of excitation in superfluid nuclei through particle-vibration coupling: Quantitative account of the variety of nuclear structure observables. *Phys. Rev. C* **2015**, *92*, 031304. [CrossRef]
97. Nomura, K.; Jolie, J. Structure of even-even cadmium isotopes from the beyond-mean-field interacting boson model. *Phys. Rev. C* **2018**, *98*, 024303. [CrossRef]
98. Sun, Z.H.; Hagen, G.; Jansen, G.R.; Papenbrock, T. Effective shell-model interaction for nuclei "southeast" of ^{100}Sn. *Phys. Rev. C* **2021**, *104*, 064310. [CrossRef]
99. De-Shalit, A.; Talmi, I.; Wigner, E.P. Review of "Nuclear Shell Theory". In *Historical and Biographycal Reflections and Syntheses*; Mehra, J., Ed.; Springer: Berlin/Heidelberg, Germany, 2001; pp. 494–495. [CrossRef]
100. Mach, H.; Korgul, A.; Górska, M.; Grawe, H. Ultrafast-timing lifetime measurements in ^{94}Ru and ^{96}Pd: Breakdown of the seniority scheme in N = 50 iso-tones. *Phys. Rev. C* **2017**, *95*, 014313. [CrossRef]
101. National Nuclear Data Center, NuDat 3. Available online: https://www.bnl.gov/world/ (accessed on 1 August 2021).
102. Jin, S.Y.; Wang, S.T.; Lee, J.; Corsi, A.; Wimmer, K.; Browne, F.; Chen, S.; Cortés, M.L.; Doornenbal, P.; Koiwai, T.; et al. Spectroscopy of ^{98}Cd by two-nucleon removal from ^{100}In. *Phys. Rev. C* **2021**, *104*, 024302. [CrossRef]
103. Qi, C. Partial conservation of seniority and its unexpected influence on E2 transitions in $g_{9/2}$ nuclei. *Phys. Lett. B* **2017**, *773*, 616. [CrossRef]
104. Pérez-Vidal, R.M. Collectivity along *N*=50: Nuclear Structure studies on the neutron-magic nuclei ^{92}Mo and ^{94}Ru with AGATA and VAMOS++. Ph.D. Thesis, Universidad de Valencia, València, Spain, 2019. Available online: https://roderic.uv.es/handle/10550/72450 (accessed on 1 November 2021).
105. Das, B.; Cederwall, B.; Qi, C.; Górska, M.; Regan, P.H.; Aktas, Ö.; Albers, H.M.; Banerjee, A.; Chishti, M.M.R.; Gerl, J.; et al. Nature of seniority symmetry breaking in the semimagic nucleus ^{94}Ru. *Phys. Rev. C, in print*.
106. Lorusso, G.; Becerril, A.; Amthor, A.; Baumann, T.; Bazin, D.; Berryman, J.; Brown, B.; Cyburt, R.; Crawford, H.; Estrade, A.; et al. Half-lives of ground and isomeric states in ^{97}Cd and the astrophysical origin of ^{96}Ru. *Phys. Lett. B* **2011**, *699*, 141–144. [CrossRef]
107. Robinson, S.J.Q.; Hoang, T.; Zamick, L.; Escuderos, A.; Sharon, Y.Y. Shell model calculations of *B(E2)* values, static quadrupole moments, and *g* factors for a number of $N = Z$ nuclei. *Phys. Rev. C* **2014**, *89*, 014316. [CrossRef]
108. Kingan, A.; Zamick, L. Odd-J states of isospin zero and one for 4-nucleon systems: Near-degeneracies. *Phys. Rev. C* **2018**, *98*, 014301. [CrossRef]
109. Fu, G.J.; Cheng, Y.Y.; Zhao, Y.M.; Arima, A. Shell model study of $T = 0$ states for ^{96}Cd by the nucleon-pair approximation. *Phys. Rev. C* **2016**, *94*, 024336. [CrossRef]
110. Nara Singh, B.S.; Liu, Z.; Wadsworth, R.; Grawe, H.; Brock, T.S.; Boutachkov, P.; Braun, N.; Blazhev, A.; Górska, M.; Pietri, S.; et al. 16+ spin-gap isomer in ^{96}Cd. *Phys. Rev. Lett.* **2011**, *107*, 172502. [CrossRef]
111. Zerguine, S.; Van Isacker, P. Spin-aligned neutron-proton pairs in $N = Z$ nuclei. *Phys. Rev. C* **2011**, *83*, 064314. [CrossRef]
112. Xu, Z.; Qi, C.; Blomqvist, J.; Liotta, R.; Wyss, R. Multistep shell model description of spin-aligned neutron–proton pair coupling. *Nucl. Phys. A* **2012**, *877*, 51–58. [CrossRef]
113. Qi, C.; Blomqvist, J.; Bäck, T.; Cederwall, B.; Johnson, A.; Liotta, R.J.; Wyss, R. Spin-aligned neutron-proton pair mode in atomic nuclei. *Phys. Rev. C* **2011**, *84*, 021301. [CrossRef]
114. Van Isacker, P. Neutron–proton pairs in nuclei. *Int. J. Mod. Phys.* **2013**, *E22*, 1330028. [CrossRef]
115. Marginean, N.; Bucurescu, D.; Alvarez, C.R.; Ur, C.A. Delayed alignments in the $N = Z$ nuclei ^{84}Mo and ^{88}Ru. *Phys. Rev. C* **2002**, *65*, 051303. [CrossRef]
116. Sun, Y. Projected shell model study on nuclei near the $N = Z$ line. *Eur. Phys. J. A* **2003**, *20*, 133–138. [CrossRef]
117. Sun, Y.; Sheikh, J. Anomalous rotational alignment in $N = Z$ nuclei and residual neutron-proton interaction. *Phys. Rev. C* **2001**, *64*, 162031302. [CrossRef]
118. Kaneko, Y.S.K.; de Angelis, G. Enhancement of high-spin collectivity in $N = Z$ nuclei by the isoscalar neutron–proton pairing. *Nucl. Phys. A* **2017**, *957*, 144. [CrossRef]
119. Kaneko, Y.S.K.; Mizusaki, T.; Sun, Y.; Tazaki, S. Toward a unified realistic shell-model Hamiltonian with the mono-pole-based universal force. *Phys. Rev. C* **2014**, *89*, 011302. [CrossRef]
120. Fu, G.J.; Johnson, C.W. Nucleon-pair approximation for nuclei from spherical to deformed regions. *Phys. Rev. C* **2021**, *104*, 024312. [CrossRef]
121. Corsi, A.; Obertelli, A.; Doornenbal, P.; Nowacki, F.; Sagawa, H.; Tanimura, Y.; Aoi, N.; Baba, H.; Bednarczyk, P.; Boissinot, S.; et al. Spectroscopy of nuclei around ^{100}Sn populated via two-neutron knockout reactions. *Phys. Rev. C* **2018**, *97*, 044321. [CrossRef]

122. Banu, A.; Gerl, J.; Fahlander, C.; Górska, M.; Grawe, H.; Saito, T.R.; Wollersheim, H.-J.; Caurier, E.; Engeland, T.; Gniady, A.; et al. ^{108}Sn studied with intermediate-energy Coulomb excitation. *Phys. Rev. C* **2005**, *72*, 061305. [CrossRef]
123. Maheshwari, B. A unified view of the first-excited 2^+ and 3^- states of Cd, Sn and Te isotopes. *Eur. Phys. J. Spéc. Top.* **2020**, *229*, 2485–2495. [CrossRef]
124. Guastalla, G.; DiJulio, D.D.; Górska, M.; Cederkall, J.; Boutachkov, P.; Golubev, P.; Pietri, S.; Grawe, H.; Nowacki, F.; Sieja, K.; et al. Coulomb Excitation of ^{104}Sn and the Strength of the ^{100}Sn Shell Closure. *Phys. Rev. Lett.* **2013**, *110*, 172501. [CrossRef]
125. Jonsson, N.-G.; Bäcklin, A.; Kantele, J.; Julin, R.; Luontama, M.; Passoja, A. Collective states in even Sn nuclei. *Nucl. Phys. A* **1981**, *371*, 333–348. [CrossRef]
126. Vaman, C.; Andreoiu, C.; Bazin, D.; Becerril, A.; Brown, B.A.; Campbell, C.M.; Chester, A.; Cook, J.M.; Dinca, D.C.; Gade, A.; et al. Z = 50 shell gap near ^{100}Sn from intermediate-energy Coulomb excitations in even-mass $^{106–112}$Sn isotopes. *Phys. Rev. Lett.* **2007**, *99*, 162501. [CrossRef]
127. Cederkall, J.; Ekstrom, A.; Fahlander, C.; Hurst, A.M.; Hjorth-Jensen, M.; Ames, F.; Banu, A.; Butler, P.A.; Davinson, T.; Pramanik, U.D.; et al. Sub-barrier Coulomb excitation of ^{110}Sn and its implications for the ^{100}Sn shell closure. *Phys. Rev. Lett.* **2007**, *98*, 172501. [CrossRef]
128. Ekström, A.; Cederkäll, J.; Fahlander, C.; Hjorth-Jensen, M.; Ames, F.; Butler, P.A.; Davinson, T.; Eberth, J.; Fincke, F.; Görgen, A.; et al. $0^+_{gs} \rightarrow 2^+_1$ transition strengths in ^{106}Sn and ^{108}Sn. *Phys. Rev. Lett.* **2008**, *101*, 012502. [CrossRef]
129. Orce, J.N.; Choudry, S.N.; Crider, B.; Elhami, E.; Mukhopadhyay, S.; Scheck, M.; McEllistrem, M.T.; Yates, S.W. $2^+_1 \rightarrow 0^+_1$ transition strengths in Sn nuclei. *Phys. Rev. C* **2007**, *76*, 021302. [CrossRef]
130. Bader, V.M.; Gade, A.; Weisshaar, D.; Brown, B.A.; Baugher, T.; Bazin, D.; Berryman, J.S.; Ekstrom, A.; Hjorth-Jensen, M.; Stroberg, R.; et al. Quadrupole collectivity in neutron-deficient Sn nuclei: ^{104}Sn and the role of proton excitations. *Phys. Rev. C* **2013**, *88*, 051301. [CrossRef]
131. Doornenbal, P.; Reiter, P.; Grawe, H.; Wollersheim, H.J.; Bednarczyk, P.; Caceres, L.; Cederkäll, J.; Ekström, A.; Gerl, J.; Górska, M.; et al. Enhanced strength of the $2^+_1 \rightarrow 0^+_{gs}$ transition in ^{114}Sn studied via Coulomb excitation in inverse kinematics. *Phys. Rev. C* **2008**, *78*, 031303. [CrossRef]
132. Kumar, R.; Doornenbal, P.; Jhingan, A.; Bhowmik, R.K.; Muralithar, S.; Appannababu, S.; Garg, R.; Gerl, J.; Górska, M.; Kaur, J.; et al. Enhanced $0^+_{gs} \rightarrow 2^+_1$ $E2$ transition strength in ^{112}Sn. *Phys. Rev. C* **2010**, *81*, 024306. [CrossRef]
133. Kumar, R.; Saxena, M.; Doornenbal, P.; Jhingan, A.; Banerjee, A.; Bhowmik, R.K.; Dutt, S.; Garg, R.; Joshi, C.; Mishra, V.; et al. No evidence of reduced collectivity in Coulomb-excited Sn isotopes. *Phys. Rev. C* **2017**, *96*, 054318. [CrossRef]
134. Allmond, J.M.; Radford, D.C.; Baktash, C.; Batchelder, J.C.; Galindo-Uribarri, A.; Gross, C.J.; Hausladen, P.; Lagergren, K.; LaRochelle, Y.; Padilla-Rodal, E.; et al. Coulomb excitation of ^{124,126,128}Sn. *Phys. Rev. C* **2011**, *84*, 061303. [CrossRef]
135. Allmond, J.M.; Stuchbery, A.E.; Galindo-Uribarri, A.; Padilla-Rodal, E.; Radford, D.C.; Batchelder, J.C.; Bingham, C.R.; Howard, M.E.; Liang, J.F.; Manning, B.; et al. Investigation into the semimagic nature of the tin isotopes through electromagnetic moments. *Phys. Rev. C* **2015**, *92*, 041303. [CrossRef]
136. Jungclaus, A.; Walker, J.; Leske, J.; Speidel, K.-H.; Stuchbery, A.; East, M.; Boutachkov, P.; Cederkall, J.; Doornenbal, P.; Egido, J.L.; et al. Evidence for reduced collectivity around the neutron mid-shell in the stable even-mass Sn isotopes from new lifetime measurements. *Phys. Lett. B* **2011**, *695*, 110–114. [CrossRef]
137. Kumbartzki, G.J. Transient field g factor and mean-life measurements with a rare isotope beam of ^{126}Sn. *Phys. Rev. C* **2012**, *86*, 034319. [CrossRef]
138. Kumbartzki, G.J.; Benczer-Koller, N.; Speidel, K.-H.; Torres, D.A.; Allmond, J.M.; Fallon, P.; Abramovic, I.; Bernstein, L.A.; Bevins, J.E.; Crawford, H.; et al. Z = 50 core stability in ^{110}Sn from magnetic-moment and lifetime measurements. *Phys. Rev. C* **2016**, *93*, 044316. [CrossRef]
139. Doornenbal, P.; Takeuchi, S.; Aoi, N.; Matsushita, M.; Obertelli, A.; Steppenbeck, D.; Wang, H.; Audirac, L.; Baba, H.; Bednarczyk, P.; et al. Intermediate-energy Coulomb excitation of ^{104}Sn: Moderate $E2$ strength decrease approaching ^{100}Sn. *Phys. Rev. C* **2014**, *90*, 061302. [CrossRef]
140. Radford, D.C.; Baktash, C.; Barton, C.J.; Batchelder, J.; Beene, J.R.; Bingham, C.R.; Caprio, M.A.; Danchev, M.; Fuentes, B.; Galindo-Uribarri, A.; et al. Coulomb excitation and transfer reactions with neutron-rich radioactive beams. *Int. Conf. Exot. Nucl. At. Masses* **2005**, *746*, 383–387. [CrossRef]
141. Radford, D.; Baktash, C.; Barton, C.; Batchelder, J.; Beene, J.; Bingham, C.; Caprio, M.; Danchev, M.; Fuentes, B.; Galindo-Uribarri, A.; et al. Coulomb excitation and transfer reactions with rare neutron-rich isotopes. *Nucl. Phys. A* **2005**, *752*, 264–272. [CrossRef]
142. Spieker, M.; Petkov, P.; Litvinova, E.; Müller-Gatermann, C. Shape coexistence and collective low-spin states in ^{112,114}Sn studied with the (p, p'γ) Doppler-shift at-tenuation coincidence technique. *Phys. Rev. C* **2018**, *97*, 054319. [CrossRef]
143. Berger, M. Kernstrukturuntersuchungen bis zur Teilchenseparationsschwelle mit der Methode der Kernresonanzfluoreszen. Ph.D. Thesis, Technical University of Darmstadt, Darmstadt, Germany, 2020. [CrossRef]
144. Rosiak, D.; Seidlitz, M.; Reiter, P.; Naïdja, H.; Tsunoda, Y.; Togashi, T.; Nowacki, F.; Otsuka, T.; Colò, G.; Arnswald, K.; et al. Enhanced quadrupole and octupole strength in doubly magic ^{132}Sn. *Phys. Rev. Lett.* **2018**, *121*, 252501. [CrossRef]
145. Coraggio, L.; Covello, A.; Gargano, A.; Itaco, N.; Kuo, T.T.S. Shell-model study of quadrupole collectivity in light tin isotopes. *Phys. Rev. C* **2015**, *91*, 041301. [CrossRef]
146. Cortes, L.M. (INFN Legnro, Italy). Data analysis of the Coulomb excitations of ^{102}Sn experiment. Private communication, 2021.

147. Wimmer, K. (GSI Darmstadt, Germany). Review submitted to Prog. Part. Nucl. Phys. Private communication, 2021.
148. Siciliano, M.; Valiente-Dobón, J.J.; Goasduff, A.; Rodríguez, T.R.; Bazzacco, D.; Benzoni, G.; Braunroth, T.; Cieplicka-Oryńczak, N.; Clément, E.; Crespi, F.C.L.; et al. Lifetime measurements in the even-even $^{102–108}$Cd isotopes. *Phys. Rev. C* **2021**, *104*, 034320. [CrossRef]
149. Górska, M.; Lipoglavsek, M.; Grawe, H.; Nyberg, J.; Atac, A.; Axelsson, A.; Bark, R.; Blomqvist, J.; Cederkäll, J.; Cederwall, B.; et al. $^{98}_{48}Cd_{50}$: The two-proton-hole spectrum in $^{100}_{50}Sn_{50}$. *Phys. Rev. Lett.* **1997**, *79*, 2415. [CrossRef]